Chemical Engineering Science 147 (2016) 1–12

Contents lists available at ScienceDirect

Chemical Engineering Science

journal homepage: www.elsevier.com/locate/ces

A multi-region model for reaction–diffusion process within a porous catalyst pellet

Hua Li, Mao Ye *, Zhongmin Liu

Dalian National Laboratory for Clean Energy, National Engineering Laboratory for MTO, iChEM (Collaborative Innovation Center of Chemistry for Energy Materials), Dalian Institute of Chemical Physics, Chinese Academy of Sciences, 457 Zhongshan Road, Dalian 116023, China

HIGHLIGHTS

- A meso-scale multi-region model is developed for a single porous catalyst pellet.
- The numerical methods are proposed for multi-scale reaction–diffusion problems.
- The model is validated against the alkylation of benzene over H-ZSM-5 crystal particles.
- The effects of volume fraction, size, and spatial distribution of H-ZSM-5 crystal particles are studied.

ARTICLE INFO

Article history:
Received 24 August 2015
Received in revised form
29 February 2016
Accepted 1 March 2016
Available online 8 March 2016

Keywords:
Catalyst
Reaction–diffusion
Multi-region model
Meso-scale

ABSTRACT

In this paper, a multi-region model based on the unified Maxwell–Stefan diffusion theory is developed to investigate the reaction–diffusion processes within catalyst pellets formed by micro-pore particles and meso/macro-pore support. The corresponding partial differential equation (PDE) systems, describing chemical reactions, bulk diffusion, Knudsen diffusion, surface diffusion and viscous flow, are converted to ODE systems based on finite volume method (FVM). The resulting multi-scale ODE systems are solved by reduced storage matrix method, where a quasi-stationary state assumption is adopted in the numerical solution to solve multi-scale problem in which the diffusivities of micro-pores and meso/macro-pores are significantly different. The alkylation of benzene over a single multi-porous pellet formed with H-ZSM-5 crystal particles was simulated as an example. The effects of volume fraction, size and spatial distribution of H-ZSM-5 crystal particles on the effectiveness factor of the catalyst pellet were then investigated and discussed. It is shown that the multi-region model is a potential bottom to up tool for reaction–diffusion processes in catalyst pellet exhibiting multi-scale time characteristic.

1. Introduction

Zeolite catalysts see their applications in a variety of industrial sectors including, among others, fluid catalytic cracking (FCC) and methanol to olefins (MTO). Despite the complex mass and heat transfer between catalyst pellets and surrounding fluid, the performance of single catalyst pellet affects the reactor operation significantly. The latter is strongly dependent upon the transport phenomena inside the catalyst pellet, such as reactants adsorption, multi-component diffusion, surface reaction, and reactants and products desorption (Keil, 2012, 2013). Practically zeolite catalyst pellets used in industrial reactors have complicated porous structures, in which pores with different sizes may co-exist. For instance, an industrial MTO catalyst pellet is composed of micro-pore SAPO-34 zeolite crystal particles and macro/meso-pore catalyst support (or called matrix). Here the micro-pores refer to the pores smaller than 2 nm, the macro-pores refer to those larger than 50 nm, and the meso-pores are in between (Krishna, 1993; Krishna and Wesselingh, 1997). The same can be found in industrial FCC catalyst pellet where the micro-pore Y zeolite crystal particles are surrounded by macro/meso-pore catalyst support. The study of reaction and molecular diffusion in the micro-pore zeolite crystals has received considerable interest in past decades (Kärger and Ruthven, 1992; Chen et al., 1994). However, despite the diffusion-reaction process inside the zeolite crystals, the transport and thus the reaction in an industrial zeolite catalyst pellet are also highly related to the number, position, and size distribution of the micro-pore zeolite crystal particles. Previous studies found that the effectiveness factor of a single micro-pore crystal particle decreases as the particle size increases due to the diffusion limitations (Hansen et al., 2009).

* Corresponding author.
E-mail address: maoye@dicp.ac.cn (M. Ye).

http://dx.doi.org/10.1016/j.ces.2016.03.004
0009-2509/

As the diffusion coefficients (the bulk diffusion combined with Knudsen diffusion) in the macro/meso-pores may be 4–6 orders of magnitude higher than that of surface diffusion in the micro-pores, it is usually assumed that the macro/meso-pores do not significantly affect intracrystalline diffusion, and only a few studies concerning the transport of reactants and products in macro/meso-pores in the catalyst support have been reported so far in the open literature (Hinderer and Keil, 1995; Keil et al., 1999). A series of experimental studies by Kortunov et al., (2005) showed that the diffusion in macro/meso-pores in fact plays an important role in the transport inside catalyst pellets. In this connection, in order to improve the diffusivity of reactants and products and thus enhance the reaction rates in the catalyst pellet, the number, position, and size distribution of micro-pore crystal l particles have to be optimized by considering the diffusion in both macro/meso-pores and micro-pores simultaneously. Currently researchers and engineers mainly use the trial and error method to optimize the catalyst based on the conversion and selectivity data obtained in the laboratory scale experiments, which certainly elaborates the process of catalyst development. Apparently the understanding of the transport and thus reaction in real industrial catalyst pellet still requires significant effort. As the first step toward this ambition, the aim of this paper is to develop a modeling approach in which the diffusion in both micro-pores and macro/meso-pores can be studied simultaneously.

Obviously, the modeling approach capable of addressing the diffusion-reaction process in both micro-pores and macro/meso-pores simultaneously has to deal with different diffusion mechanisms dwelled in different pore sizes. From the view of modeling hierarchy, this model could be regarded as a meso-scale model (medium level). In the literature, though a variety of modeling approaches have been developed for the diffusion-reaction process in a catalyst pellet, there are few meso-scale models for catalyst pellets (Hansen et al., 2009; Solsvik and Jakobsen, 2012). Most models could be ascribed to micro-scale and macro-scale models. Micro-scale models are at the lowest level for catalyst particles, their research objects focus only on zeolite crystals. Keil (2012) and Hansen and Keil (2012) recently proposed a hierarchical modeling strategy for diffusion-reaction process in zeolite crystals, in which the first principles, quantum chemistry, force field simulations and macroscopic differential equations are coupled at different scales. In their strategy, the quantum chemical calculations is applied to study the influence of the active sites of the catalyst, which is followed by Monte Carlo and molecular dynamic simulations of adsorption and diffusion of reactants and products, and ended with continuum modeling of zeolite particles. The main idea in this micro-scale model is to use the results obtained in the simulations at a lower level as an input to the simulations at a higher level. This comprehensive modeling strategy has been demonstrated in the analysis of the diffusion limitation in the alkylation of benzene over H-ZSM-5 crystals (Hansen et al., 2009). Macro-scale models are at highest level for catalyst particles. The main feature of this model is to assume uniform distribution of reaction sites and the same diffusion mechanism inside the whole catalyst particle. In the real catalytic reactors, the reactions over the catalyst pellets are complicated and the diffusion of multi-components needs to be taken into account. So the assumption of uniform distribution can considerably reduce the computational time. The classical approach for predicting the multi-components diffusion and reaction in catalyst pellets is to employ continuum equations with the assumption of the uniform distribution of pore size and active sites in the catalyst pellet (Sahimi, 1990; Hegedus and Pereira, 1990; Solsvik and Jakobsen, 2011, 2012; Keil, 2012; Lim and Dennis, 2012). Solsvik and Jakobsen (2012) recently outlined the derivation of the different diffusion flux models for porous pellets with respect to the molar based and the mass based average velocity definition. The diffusion resistances described by the macro-scale continuum models are in essence the effective resistances which account for the comprehensive effect of the steric resistance and adsorption introduced by the existence of micro-pore crystal particles (active sites). The reaction rates in the continuum models, on other hand, are related to the effective rates where the diffusion within the micro-pore crystal particles is neglected. Therefore, the main problem for macro-scale models is how to effectively predict the diffusion and rate parameters. The key lies in meso-scale models. Since the micro-scale model is related with elementary reaction steps, a meso-scale model embodies important theoretical significance in linking the micro-scale model and macro-scale model.

A meso-scale model could deal with different diffusion mechanisms for different pore sizes. For micro-pore crystal particles, surface diffusion of adsorbed molecular components along the pore wall surface is dominant. The adsorption isotherms and diffusion coefficients within micro-pores could be effectively predicted by means of molecular dynamics and Monte Carlo simulations (Hansen et al., 2009; Hansen and Keil, 2012; Smit and Maesen, 2008). While for macro/meso-pores, the bulk (or molecular) diffusion and Knudsen diffusion becomes important suppose that no strong adsorption exists. In addition, the pressure gradient inside the pellet is not negligible if there is a net change in the number of moles inside the porous catalyst, which can lead to the viscous or Darcy flow in the pellet (Krishna, 1993; Krishna and Wesselingh, 1997). The fluxes of bulk and Knudsen diffusion as well as the viscous flow can be described by a modified Maxwell–Stefan model (Krishna and van Baten, 2009a) in which the gas-phase Maxwell–Stefan diffusion model is modified by introducing the interaction between the species and pore surface or wall. Therefore, it is possible to derive a unified Maxwell–Stefan description for diffusion and/or viscous flow for both micro- and meso-/macro-pores, as shown by Krishna and van Baten (2009b). The main problem for this approach caused by the difference of the diffusion coefficients between macro/meso-pores and micro-pores could be at several orders of magnitude, which means that the diffusion resistance, and thus the characteristic time could be significantly different for these different size pores. In current contribution, we develop a numerical scheme to address this problem.

This paper is organized as following: firstly the unified Maxwell–Stefan diffusion theory is used to describe diffusion and reaction behavior in both micro- and macro/meso-pores in catalyst pellets. Then the multi-region model and corresponding numerical methods are introduced. This model is validated against the results of alkylation of benzene over a single multi-porous pellet formed with H-ZSM-5 crystal particles by Hansen et al. (2009). Finally, the effects of volume fraction, size, and spatial distribution of the H-ZSM-5 crystal particles on the effectiveness factor are studied and discussed.

2. Modeling

2.1. Multi-region model

Our model for reaction–diffusion process in catalyst pellet with multi-pores is a natural outcome of the hierarchical multi-scale idea. From theoretical view, the use of quantum chemical or *ab initio* dynamical simulation can give deep insight into details of a catalytic reaction process with high accuracy. However, the quantum chemical approach, due to its time-consuming characteristic, has been mostly used to calculate energy barriers of elementary reactions and vibration frequency spectrum of stationary geometries along the reaction coordinate (Keil, 2012; Hansen and Keil, 2012). The limited time and length scales in quantum chemical calculation hinder its application in catalyst

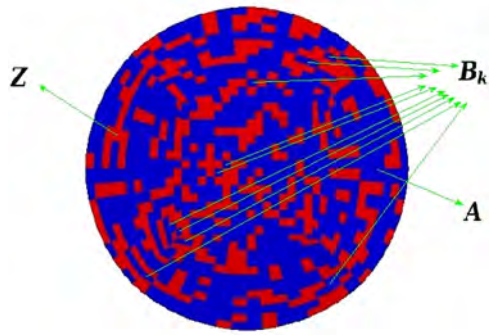

Fig. 1. A catalyst pellet formed with micro-pore crystal particles region $\mathcal{Z}$ and support region $\mathcal{S}$. The region $\mathcal{S}$ is decomposed into subregion $\mathcal{A}$ and $\mathcal{B}_k$.

design and reactor optimization. A model based on hierarchical multi-scale idea is more practical for real application.

A single catalyst pellet could be decomposed into two different types of regions: micro-pore crystal region $\mathcal{Z}$and catalyst support (or matrix) region $\mathcal{S}$. It is assumed that only the micro-pore crystals contain the active sites of the catalyst, where the reactions and surface diffusions may occur. The catalyst support consists of meso-pores or macro-pores, where the bulk diffusion combined with Knudsen diffusion dominate if no strong adsorption exists. Generally, the difference of the diffusion coefficients between these two types of regions is about several orders of magnitude, which means that the diffusion resistance and thus the characteristic time is significantly different for regions $\mathcal{Z}$ and $\mathcal{S}$. The convenient approach for solving such problem is to describe the reaction–diffusion process in the whole particle by two separate partial differential equations (PDEs) that are coupled with component mass fluxes.

Surface reactions around micro-pore crystals are always not negligible because of high transport ability of the support region. It is natural to incorporate the surface reaction term into the PDE for catalyst support region $\mathcal{S}$. However, the different characteristic time between the diffusion and surface reaction may lead to the solution much more complicated. In fact, according to whether it connects to the external boundary of the catalyst pellet or not, the catalyst support region $\mathcal{S}$ can be decomposed into two different types of subregions: $\mathcal{A}$ and $\mathcal{B}$. $\mathcal{A}$denotes the subregion connected to the external boundary of the pellet, and $\mathcal{B}$ denotes the subregion that is not directly connected to the external boundary. The subregion $\mathcal{B}$ can be further divided into small regions $\mathcal{B}_k$ (k=1, 2, 3, …, M) due to the connectivity, i.e., each region $\mathcal{B}_k$ is isolated by support region $\mathcal{Z}$. Fig. 1 shows a simplified two-dimension partition for illustrating the hierarchical relation for different types of regions. Let us now ignore the coupling between the support region and the zeolite crystal region for simplification. If the diffusion transfer is considerably faster than the surface reaction kinetics, the exchange rate of component masses between subregion $\mathcal{A}$ and environment of the catalyst pellet will be much faster than the rate of the surface reaction. However, in each small region $\mathcal{B}_k$ the faster diffusion transfer only increase the speed in achieving the uniform distribution of components of interest, and the surface reaction rate determines the speed in achieving the stationary state of small region $\mathcal{B}_k$. This implies that the subregion $\mathcal{B}$ will need a much longer time than that of the subregion $\mathcal{A}$ to approach stationary state. So it is meaningful to further separate the PDE system of the catalyst support region $\mathcal{S}$ according to its region connectivity.

The catalyst pellet formed with the randomly distributed micro-pore crystals could be split into micro-pore crystal region $\mathcal{Z}$, subregion $\mathcal{A}$, and subregion $\mathcal{B}_k$(k=1, 2, 3, …, M) based on the discussion above. Each region is controlled by its own PDEs with coupling boundary conditions. We call such scheme *multi-region model*. When volume fraction of subregion $\mathcal{B}$ is small, the subregion $\mathcal{B}$ could be replaced by micro-pore crystals for simplification, and the effect of the replacement in analyzing catalytic performance of the pellet will be negligible.

2.1.1. Continuum approach for micro-porous crystal region $\mathcal{Z}$

The change of loading of component i with time in the region $\mathcal{Z}$ due to reaction and diffusion is described by the following PDEs:

$$\frac{\partial q_i}{\partial t} = -\nabla\cdot\vec{N_i} + r_i \quad (i = 1,2, \ldots, n) \tag{1}$$

where q_i (in $\frac{\text{molecules}}{\text{unit cell}}$) is the loading of component i, $\vec{N_i}$(in $\frac{\text{m}}{\text{s}}\frac{\text{molecules}}{\text{unit cell}}$) the molecular flux of component i, r_i (in $\frac{1}{\text{s}}\frac{\text{molecules}}{\text{unit cell}}$) the reaction rate of component i, and t (in s) the time.

The flux of component i, $\vec{N_i}$, is predicted based on the Maxwell–Stefan diffusion theory. The equations for *n*-component diffusion can be written as follow (Hansen et al. 2009)

$$-\frac{\theta_i}{RT}\nabla\mu_i = \sum_{\substack{j=1\\ j\neq i}}^{n}\frac{q_j\vec{N_i} - q_i\vec{N_j}}{q_i^{sat}q_j^{sat}\mathcal{D}_{ij}} + \frac{\vec{N_i}}{q_i^{sat}\mathcal{D}_i} \quad (i = 1,2, \ldots, n) \tag{2}$$

where μ_i (in $\frac{\text{J}}{\text{kmol}}$) is the molar chemical potential of component *i*, R (in $\frac{\text{J}}{\text{kmol K}}$) the gas constant, T (in K) the absolute temperature, q_i^{sat} (in $\frac{\text{molecules}}{\text{unit cell}}$) the saturation loading of component i, $\mathcal{D}_i$ (in $\frac{\text{m}^2}{\text{s}}$) the Maxwell-Stefan diffusivity of component i, $\mathcal{D}_{ij}$ (in $\frac{\text{m}^2}{\text{s}}$) the exchange coefficient between component i and j, and θ_i(in dimensionless) the fractional occupancies of component i which is defined as $\theta_i \equiv \frac{q_i}{q_i^{sat}}$. The form of Maxwell–Stefan equation, Eq. (2), is slightly different from that in Hansen et al. (2009) by defining $\vec{N_i} \equiv q_i\vec{u_i}$ here, where $\vec{u_i}$ (in $\frac{\text{m}}{\text{s}}$) is the velocity of component i. The gradient of the chemical potential can be expressed in terms of thermodynamic correction factors, Γ_{ij}(in dimensionless), and the gradient in q_i (Hansen et al., 2009),

$$\frac{q_i}{RT}\nabla\mu_i = \sum_{j=1}^{n}\Gamma_{ij}\nabla q_j,\ \Gamma_{ij} \equiv \frac{q_i}{q_j}\frac{\partial \ln f_i}{\partial \ln q_j} = \frac{q_i}{f_i}\frac{\partial f_i}{\partial q_j} \quad (i,j = 1,2, \ldots, n) \tag{3}$$

where f_i (in Pa) denotes the partial fugacity of component i. The relation between f_i and q_i can be obtained on the basis of multi-component adsorption theory, e.g. the ideal adsorbed solution theory (IAST) (Myers and Prausnitz, 1965). The solution of Eqs. (2) and (3) for the fluxes is given by

$$\begin{pmatrix}\vec{N_1}\\ \vec{N_2}\\ \cdots\\ \vec{N_n}\end{pmatrix} = -[B]^{-1}[\Gamma]\begin{pmatrix}\nabla q_1\\ \nabla q_2\\ \cdots\\ \nabla q_n\end{pmatrix} \tag{4}$$

where the elements of matrix $[\Gamma]$ are defined in Eq. (3), and elements of matrix [B] are

$$B_{ii} = \frac{1}{\mathcal{D}_i} + \sum_{\substack{j=1\\ j\neq i}}^{n}\frac{\theta_j}{\mathcal{D}_{ij}},\ B_{ij(i\neq j)} = -\frac{q_i^{sat}}{q_j^{sat}}\frac{\theta_i}{\mathcal{D}_{ij}} (i,j = 1,2,\ldots,n) \tag{5}$$

Eqs. (1) and (4) describe the reaction–diffusion processes in micro-pore crystals. The parameters $\mathcal{D}_i$, $\mathcal{D}_{ij}$ and Γ_{ij}can be predicted based on the molecular dynamic simulations and Monte Carlo simulations. And the parameters of reaction kinetics can be obtained by quantum chemical calculations in combination with harmonic transition state theory. The Maxwell–Stefan diffusion model combined with multi-component adsorption theory provides a quantitative prediction of the multi-component fluxes in the micro-pore crystals.

2.1.2. Continuum approach for subregion $\mathcal{A}$ of catalyst support region

The governing equations of component mass balance in the catalyst support region $\mathcal{S}$ could be described as follow

$$\epsilon\frac{\partial c_i}{\partial t} = -\nabla\cdot\vec{\mathbb{N}}_i + \mathbb{r}_i \ (i=1,2,\ldots,n) \tag{6}$$

where ϵ (in dimensionless) denotes porosity of catalyst support, c_i (in $\frac{kmol}{m^3}$) the concentration of component i, $\overrightarrow{\mathbb{N}_i}$ (in $\frac{m}{s}\frac{kmol}{m^3}$) the molar flux of component i, and $\mathbb{r}_i$ (in $\frac{1}{s}\frac{kmol}{m^3}$) the reaction rate of component i. The value of $\mathbb{r}_i$ in the support region is zero if the surface reactions are ignored. When the surface reactions are not ignored, $\mathbb{r}_i$ can be calculated by

$$\mathbb{r}_i = \frac{r_i S c_u^s}{v_c} \tag{7}$$

when the cells of interest are adjacent to the micro-pore crystals, which will be otherwise set to zero. The surface reaction refers to the reaction at the active sites that are located at the boundary face of the crystal particles, where the reaction species may be transported much faster than that inside the zeolite channel. The surface reaction is introduced to account for this effect. In the Eq. (7), S (in m^2) is the interface area between region $\mathcal{S}$ and region $\mathcal{Z}$, v_c (in m^3) is the cell volume, and c_u^s (in $\frac{kmol\ unit\ cell}{m^2}$) denotes the number (in kmol) of unit cells of micro-pore crystals per 1 m^2 area of the interface. The right hand side of Eq. (7) is calculated based on Eq. (18), where the required component loadings are computed from IAST by assuming the first layer of active sites of crystal particle is located at the boundary surface. The value of c_u^s could be predicted based on crystal's framework parameters. The flux of component i, $\overrightarrow{\mathbb{N}_i}$, could be calculated based on Maxwell–Stefan equation (Krishna and van Baten, 2009a, 2009b) described as follows

$$-\frac{1}{RT}\nabla p_i = \sum_{\substack{j=1\\ j\neq i}}^{n}\frac{x_j\overrightarrow{\mathbb{N}_i} - x_i\overrightarrow{\mathbb{N}_j}}{\mathbb{D}_{ij}^e} + \frac{\overrightarrow{\mathbb{N}_i}}{\mathbb{D}_{iS}^e} (i=1,2,\ldots,n) \tag{8}$$

where p_i (in Pa) is the pressure of component i, x_i (in dimensionless) is molar fraction of component i, $\mathbb{D}_{ij}^e$(in $\frac{m^2}{s}$) is the effective binary pair diffusion coefficients, and $\mathbb{D}_{iS}^e$(in $\frac{m^2}{s}$) is the effective Maxwell–Stefan diffusion coefficient in the porous medium. The $\mathbb{D}_{ij}^e$, $\mathbb{D}_{iS}^e$ are related to their corresponding free space values by (Krishna and Wesselingh, 1997)

$$\mathbb{D}_{ij}^e = \frac{\epsilon}{\tau}\mathbb{D}_{ij},\ \mathbb{D}_{iS}^e = \frac{\epsilon}{\tau}\mathbb{D}_{iS} \tag{9}$$

where τ (in dimensionless) denotes the tortuosity of catalyst support, $\mathbb{D}_{ij}$ (in $\frac{m^2}{s}$) are binary pair diffusion coefficients in free space, which can be estimated from the kinetic gas theory (Solsvik and Jakobsen, 2012; Reid et al., 1987), and $\mathbb{D}_{iS}$ (in $\frac{m^2}{s}$) is the Maxwell–Stefan diffusion coefficient portraying the interaction between component i with the pore surface(s). $\mathbb{D}_{iS}$, as described by Krishna and van Baten (2009a), represents a conglomerate of the "Knudsen", "surface", and "viscous" effects. Following Kerkhof (1996) and Krishnaand van Baten (2009a), we could get the formulation by neglecting the adsorption between the component i and pore surface

$$\mathbb{D}_{iS} = \mathbb{D}_{iK} + \frac{B_0 c_i RT}{\mu_i} \tag{10}$$

$$\mathbb{D}_{iK} = \frac{d_0}{3}\sqrt{\frac{8RT}{\pi M_i}} \tag{11}$$

$$B_0 = \frac{d_0^2}{32} \tag{12}$$

where $\mathbb{D}_{iK}$ (in $\frac{m^2}{s}$) is the Knudsen diffusivity (Krishna and Wesselingh 1997), and B_0 (in m^2) the permeability of the pore, μ_i (in $\frac{kg}{ms}$) the dynamic viscosity of component i, d_0 (in m) the pore diameter, and M_i (in $\frac{kg}{kmol}$) the mass of species i. The second term on the right side of Eq. (10) represents the viscous contribution.

The solution of Eq. (8) for the fluxes, $\overrightarrow{\mathbb{N}_i}$, is given by

$$\begin{pmatrix}\overrightarrow{\mathbb{N}_1}\\ \overrightarrow{\mathbb{N}_2}\\ \cdots\\ \overrightarrow{\mathbb{N}_n}\end{pmatrix} = -\left[\mathbb{B}^e\right]^{-1}\begin{pmatrix}\frac{1}{RT}\nabla p_1\\ \frac{1}{RT}\nabla p_2\\ \cdots\\ \frac{1}{RT}\nabla p_n\end{pmatrix} \tag{13}$$

where the elements of matrix $\left[\mathbb{B}^e\right]$ are

$$\mathbb{B}_{ii}^e = \frac{1}{\mathbb{D}_{iS}^e} + \sum_{\substack{j=1\\ j\neq i}}^{n}\frac{x_j}{\mathbb{D}_{ij}^e},\ \mathbb{B}_{ij(i\neq j)}^e = -\frac{x_i}{\mathbb{D}_{ij}^e} (i,j=1,2,\ldots,n) \tag{14}$$

The relationship between p_i, and c_i follows the ideal gas law

$$p_i = c_i RT \tag{15}$$

The reaction–diffusion processes in the catalyst support region $\mathcal{S}$ can be described by (Eqs. (6) and 13). The parameters ϵ, τ, and d_0 are used to characterize the porous structure of the region in approximation. Because the values of $\mathbb{D}_{ij}^e$ are larger than $\mathcal{D}_{ij}$ by several orders of magnitude, the support region $\mathcal{S}$ will need less time than the micro-pore crystal region$\mathcal{Z}$ in approaching the stationary state. Such multi-scale phenomenon also exists within the support region $\mathcal{S}$ itself. The solving scheme for the subregion $\mathcal{A}$ could approach the solution of stationary state much faster than that for subregion $\mathcal{B}$. This scheme will be applied to improve the solving efficiency. Thus the continuum approach for subregion $\mathcal{B}$ can be simplified in the following.

2.1.3. Continuum approach for subregion $\mathcal{B}$ of catalyst support region

The subregion $\mathcal{B}$ of catalyst support is not connected to the external boundary of the pellet, and it can be further decomposed into small region $\mathcal{B}_k$ (k=1, 2, 3, …, M). Each small region $\mathcal{B}_k$ is surrounded by micro-pore crystals. When the characteristic time of diffusion in $\mathcal{B}_k$ is much smaller than that of the surface reaction, the component concentration will approach the uniform distribution within $\mathcal{B}_k$ very fast, which, however, has a slow speed in approaching the stationary state. Therefore, it is convenient to assume the uniform distribution of all components in each $\mathcal{B}_k$, which can avoid solving the PDEs, Eq. (6), at a very small time step due to the small characteristic time of diffusion. For each subregion $\mathcal{B}_k$, the Eq. (6) could be simplified as

$$\epsilon\frac{dc_i}{dt} = -\nabla\bullet\overrightarrow{\mathbb{N}_i} + \mathbb{r}_i \ (i=1,2,\ldots,n) \tag{16}$$

where $\overrightarrow{\mathbb{N}_i}$ only represent the boundary fluxes of $\mathcal{B}_k$.

The simplification is not necessary if the characteristic time of diffusion in $\mathcal{B}_k$ is comparable to that of the surface reaction, since the computational efficiency in solving the PDEs is dominated by the reaction rate term in this situation. However, the simplification could approximate results anyway due to the higher transport capacity of $\mathcal{B}_k$ against micro-pore crystals.

2.1.4. Coupling boundary conditions

At the interfaces of the region $\mathcal{Z}$ and $\mathcal{S}$, the mass fluxes of each region should be equal

$$\overrightarrow{\mathbb{N}_i} = \overrightarrow{N_i}c_u^v \ (i = 1,2,\ldots,n) \tag{17}$$

where c_u^v (in $\frac{kmol\ unit\ cell}{m^3}$) denotes the number (in kmol) of unit cells of micro-pore crystal per 1 m^3 volume.

2.2. Numerical method

As stated above, the diffusion–reaction process in each region (or subregion) is described by separate time-dependent PDEs that are coupled with mass fluxes at the interfaces. The

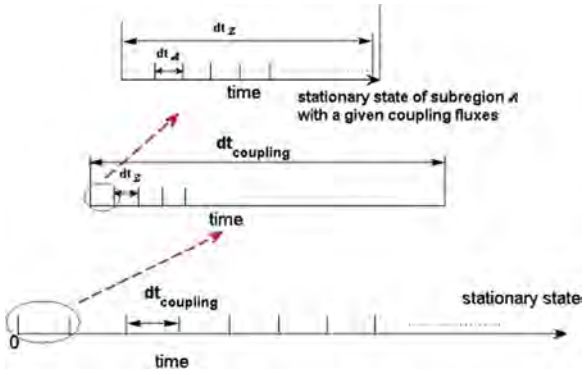

Fig. 2. Different time scales for the ODE system for reaction–diffusion inside a catalyst pellet.

time-dependent PDEs for each region (or subregion) are first discretized with respect to the spatial coordinate by use of finite volume method (FVM), which yield time-dependent ordinary differential equations (ODE) for each region (or subregion). In this work, the reduced storage matrix method (Brown and Hindmarsh, 1989), which is the combination of Newton iteration, BDF methods, GMRES iteration, and preconditioning for stiff reactions, was used to solve the stiff ODEs for each region (or subregion). For non-stiff ODEs, we replace the GMRES iteration with functional iteration and ignore the preconditioning (Brown and Hindmarsh, 1989; Radhakrishnan and Hindmarsh, 1993) such that the computational efficiency can be improved. The time step of the ODEs for each region (or subregions) is automatically controlled by presetting both the relative and absolute tolerance (Radhakrishnan and Hindmarsh, 1993; Gear, 1971).

The treatment of the boundary conditions, i.e. how to update mass fluxes at the interfaces between different regions, is critical for the computational efficiency in solving ODEs due to the multi-scale characteristics of time. The essence underlying the treatment lies in the balance between the accuracy and computational efficiency. It is obvious that a higher accuracy for the solutions of ODEs can be obtained by updating the coupled mass fluxes with a smaller time interval, which, however, leads to a much longer computational time to reach the stationary state. Fig. 2 illustrates the different time scale of the ODEs, where $dt_{coupling}$ (in s) represents the time interval for updating the coupled boundary conditions, $dt_{\mathcal{Z}}$(in s) the time step of the ODEs for region $\mathcal{Z}$, and $dt_{\mathcal{A}}$(in s) the time step of the ODEs for subregion $\mathcal{A}$. The ODEs for region $\mathcal{Z}$ and subregion $\mathcal{A}$ are solved separately at every time interval $dt_{coupling}$. Due to the different transport capacities, $dt_{\mathcal{Z}}$ may be larger than $dt_{\mathcal{A}}$ by several orders of magnitude suppose the stiff of reactions is not too large. If our interest focuses mainly on the stationary state of the catalyst pellet, or the approximate evolution of the catalyst performance, a loose solution tolerance for the ODEs for subregion $\mathcal{A}$ could be set by choosing a relatively large $dt_{coupling}$, which will in turn speed the computation to reach the stationary state of the subregion $\mathcal{A}$ with the given coupling fluxes. Another practical scheme is to set a relatively small time limit for solving the ODE system of subregion $\mathcal{A}$ at every time interval $dt_{coupling}$, and the ODE systems with the time evolution will satisfy a strict criteria and approach the stationary state of the particle at last. The choice of the time step of the ODE system of the subregions $\mathcal{B}_k$,which is not represented in Fig. 2, is determined by characteristic times of the diffusion and reactions in $\mathcal{B}_k$. It is convenient to replace the $\mathcal{B}_k$ by the micro-porous crystal when the volume of the subregion $\mathcal{B}$ is small.

Another key point in current multi-region model is to produce physical model of the catalyst pellet. In order to do that, the size of the pellet, the volume fraction of the micro-porous crystal particles, the size of the micro-porous crystal particles, and the spatial distribution of the micro-porous crystal particles need to be known *in priori*. The first step is to determine the mesh size of the pellet used in the simulations according to the size of the micro-porous crystal particles. The mesh size cannot be larger than the crystal particle size, and thus one crystal particle may include at least one unit cell of the mesh. It has to be noted that, however, the mesh of the catalyst pellet is used to solve the PDEs, and the mesh size has to be checked against the mesh convergence study of the reaction–diffusion system of the pellet. The second step is to determine how many mesh units must be included in one micro-porous crystal particle. This can be easily done as the mesh size and crystal particle size are both known. The third step is to locate the crystal particles inside the pellet. The number of the crystal particles needs to be calculated according to the size and volume fraction of the crystal particles in the pellet. Then the mesh units are grouped into *clusters*, and each *cluster* includes several neighboring mesh units and the size of the *cluster* equals the crystal particle size. Based on the spatial distribution of the crystal particles, the crystal particles will be assigned to the corresponding locations. For example, if the random spatial distribution is considered, then $N_{crystal}$ random number in the range of $1–N_{cluster}$ will be produced, where $N_{crystal}$ is the number of the micro-porous crystal particles inside the pellet, and $N_{cluster}$ is the number of *clusters*. The cluster is now defined as the crystal particle if the index of the cluster is amongst the $N_{crystal}$ random number produced above. In principle, any shape of the micro-porous crystals and the pellet could be applicable in this modeling approach, as long as suitable mesh is used.

In summary, the scheme adopted here for solving the multi-scaled problem, caused by significantly different diffusion resistance of region $\mathcal{Z}$ and $\mathcal{S}$, is based on a quasi-stationary state assumption. We exploit the different diffusivity of different regions, which leads to different speed in approaching stationary state, to improve the solving efficiency of the whole system. However, if we are only interested in steady state of the reaction–diffusion system, a steady-state solver (e.g. using Gauss Seidel iteration) is more favored since it is usually more efficient than the transient state solver.

3. Alkylation of benzene over H-ZSM-5

In the present study the multi-region model is applied to simulate the alkylation of benzene over a single multi-porous pellet formed by H-ZSM-5 crystals. The considered reaction kinetics is described by a one-step reaction scheme, and the parameters of reaction kinetics and diffusion of the H-ZSM-5 crystal region are obtained from Hansen et al. (2009). The C2H4/C6H6 ratio at the boundary of the catalyst pellet was also in accordance with that in Hansen et al. (2009). The rates of three species corresponding to the one-step mechanism are (Hansen et al., 2009)

$$-r_{C2H4} = -r_{C6H6} = r_{C8H10} = k_f \frac{q_{C6H6}}{22-3.25q_{C6H6}-3.5q_{C8H10}} q_{C2H4} \frac{q_{C6H6}}{q_{C6H6}+q_{C8H10}} \lambda - k_r q_{C8H10} \frac{q_{C8H10}}{q_{C6H6}+q_{C8H10}} \lambda \quad (18)$$

Table 1
Three-site Langmuir parameters of C_2H_4, C_6H_6 and C_8H_{10} at 653 K (Hansen et al., 2009).

Species	$\left[\frac{\text{molecules}}{\text{unit cell}}\right]$			$\left[\frac{1}{\text{Pa}}\right]$		
	$q_{i,A}^{sat}$	$q_{i,B}^{sat}$	$q_{i,C}^{sat}$	$b_{i,A}$	$b_{i,B}$	$b_{i,C}$
C_2H_4	12	5	2	8.40e−8	1.50e−9	4.46e−12
C_6H_6	4	4	4	1.97e−6	4.44e−9	7.58e−11
C_8H_{10}	4	2	0	3.13e−6	5.58e−10	0

where k_f (in $\frac{1}{s}$) and k_r (in $\frac{1}{s}$) are coefficients for the forward and reverse reaction of ethene and benzene to form ethylbenzene, respectively. The λ (in dimensionless) in Eq. (18) is the active site density (average number of acid sites per intersection) defined as $\lambda \equiv \frac{\gamma}{4}$, where γ (in dimensionless) denotes the number of protons per unit cell which are located in an intersection. We set $k_f = 6.96 \times 10^2 \frac{1}{s}$, $k_r = 1.37 \times 10^{-1} \frac{1}{s}$, corresponding to a pellet temperature of 653 K (Hansen et al., 2009) and $\lambda = 0.3425$, corresponding to 1.37 acid sites per unit cell (Hansen and Keil, 2013).

The matrix of thermodynamic correction factors, $[\Gamma]$, is calculated based on IAST (Myers and Prausnitz, 1965), only using the parameters of the pure-component adsorption equilibrium at the same temperature and the same adsorbent. According to Hansen et al. (2009), the adsorption isotherms of a pure-component are described by a three-site Langmuir model

$$q_i = \frac{q_{i,A}^{sat} b_{i,A} f_i}{1 + b_{i,A} f_i} + \frac{q_{i,B}^{sat} b_{i,B} f_i}{1 + b_{i,B} f_i} + \frac{q_{i,C}^{sat} b_{i,C} f_i}{1 + b_{i,C} f_i} \tag{19}$$

where $q_{i,X}^{sat}$ (in $\frac{\text{molecules}}{\text{unit cell}}$) denotes the saturation capacity of species i on site X (X=A, B, C), and $b_{i,X}$ (in $\frac{1}{Pa}$) is the affinity constant of species i on site X (see Table 1).

The exchange coefficients $\mathcal{D}_{ij}$ required by Eq. (2) are estimated using the interpolation formula (Hansen et al., 2009)

$$q_j^{sat} \mathcal{D}_{ij} = \left[q_j^{sat} \mathcal{D}_{ii}\right]^{\frac{q_i}{q_i + q_j}} \left[q_i^{sat} \mathcal{D}_{jj}\right]^{\frac{q_j}{q_i + q_j}} = q_i^{sat} \mathcal{D}_{ji} \tag{20}$$

The self-exchange coefficients, $\mathcal{D}_{ii}$(in $\frac{m^2}{s}$) , is related to the Maxwell–Stefan diffusivity by an empirical correlation (Hansen et al., 2009)

$$\mathcal{D}_{ii} = \mathcal{D}_i \left[a_{i,1} \exp(-a_{i,2}\theta) + a_{i,3} \exp(-a_{i,4}\theta)\right] \tag{21}$$

where $a_{i,1}$, $a_{i,2}$, $a_{i,3}$, and $a_{i,4}$ are dimensionless coefficients, θ (in dimensionless) is the total occupancy of the mixture defined as $\theta = \sum_{i=1}^{3} \theta_i$. The loading dependencies of the diffusivities of benzene and ethylbenzene are approximated by a simple relation (Hansen et al., 2009)

$$\mathcal{D}_i = \mathcal{D}_i(0)(1 - \theta) \tag{22}$$

While for ethene, an improved relation is used (Hansen et al., 2009)

$$\mathcal{D}_i = \mathcal{D}_i(0) \frac{(1+\varepsilon)^{z-1}}{(1 + \frac{\varepsilon}{f})^z} \tag{23}$$

with

$$\varepsilon = \frac{(\beta - 1 + 2\theta) f}{2(1-\theta)}, \beta = \sqrt{1 - 4\theta(1-\theta)\left(1 - \frac{1}{f}\right)}, f = a \exp(b\theta) \tag{24}$$

In Eqs. (23) and (24), z, a, and b are dimensionless parameters. Table 2 gives the values of these diffusion parameters.

4. Results and discussion

The alkylation of benzene in a catalyst pellet formed by H-ZSM-5 crystals was studied as an example by use of current multi-region model. We first validated the model by comparing the simulation results for single spherical catalyst pellets with those reported in Hansen et al. (2009). In the validation, the catalyst pellets formed exclusively by H-ZSM-5 crystals were simulated for eleven pellet sizes and three total boundary phase pressures under the fixed boundary benzene/ethene molar ratio of 5. After validation, we studied effects of volume fraction, size and spatial distribution of H-ZSM-5 crystal particles on the effectiveness factor at fixed boundary partial pressures (83316.67, 416583.33, and 100.0 Pa for C_2H_4, C_6H_6, and C_8H_{10}, respectively) for catalyst pellets of radius of 10 μm. In all simulations, the temperature is fixed at 653K. The parameters ϵ, τ, and d_0, which are used to characterize the porous structure of the region $\mathcal{S}$, are assigned as 0.5 (dimensionless), 4.0 (dimensionless), and 10 (nm), respectively. For convenience of analyzing these effects, we define two internal effective factors as follow

$$\eta_{pellet} \equiv \frac{\int_{V_\mathcal{Z}} r_{C8H10}\, dV + \frac{c_u^s}{c_u^v} \int_{S_\mathcal{Z}} r_{C8H10}\, dS}{r_{C8H10}^b V_{pellet}} \tag{25}$$

$$\eta_\mathcal{Z} \equiv \frac{\int_{V_\mathcal{Z}} r_{C8H10}\, dV + \frac{c_u^s}{c_u^v} \int_{S_\mathcal{Z}} r_{C8H10}\, dS}{r_{C8H10}^b V_\mathcal{Z}} \tag{26}$$

where $V_\mathcal{Z}$(in m^3) represents the total volume of the region $\mathcal{Z}$, and $S_\mathcal{Z}$ is the total area of the boundary faces of the region $\mathcal{Z}$, V_{pellet} (in m^3) denotes the total volume of the whole catalyst pellet, and r_{C8H10}^b (in $\frac{1}{s} \frac{\text{molecules}}{\text{unit cell}}$) is the reaction rate of ethylbenzene calculated at boundary temperature and partial pressures. For H-ZSM-5 crystal, we set

$$c_u^s = 4.1680 \times 10^{-10} \frac{\text{kmol unit cell}}{m^2}, c_u^v = 0.30950 \frac{\text{kmol unit cell}}{m^3} \tag{27}$$

Based on the (Eqs. (25) and 26), it could be found that $r_{C8H10}^b \eta_{pellet}$ means the volume mean reaction rate of catalyst pellet, and $r_{C8H10}^b \eta_\mathcal{Z}$ represents the volume mean reaction rate of crystal region $\mathcal{Z}$. The fixed boundary temperature and partial pressures means the value of r_{C8H10}^b is constant. Therefore, the curve shape of volume mean reaction rate is identical with that of its corresponding effective factor when the boundary partial pressures and temperature are fixed.

4.1. Model validation

In order to choose suitable mesh size for these simulations, effectiveness factors of a pellet of 10 μm radius that is composed exclusively by H-ZSM-5 crystals (see Fig. 3) were first calculated by setting the radial mesh size as 0.5, 0.25, 0.1667, 0.125 μm respectively. As it can be seen, when the mesh size reduces, the effectiveness factor predicted increases, which means fine mesh is preferred for accurate effectiveness factor calculation. On the other hand, however, fine mesh size means large number of mesh units, and this certainly causes much heavier computational load. A close check discovers that when the mesh size decreases from 0.25 to 0.125 μm, the effectiveness factor changes from 0.557 to 0.598, which indicates an increase of relative error of the solution of 6.75%. Note that the number of mesh units for mesh size of

Table 2
Diffusion parameters of C_2H_4, C_6H_6 and C_8H_{10} at 653 K (Hansen et al., 2009).

Species	q_i^{sat}	$\mathcal{D}_i(0)$	[dimensionless] (Eqs. (23), and (24))			[dimensionless] (Eq. (21))			
	$\left[\frac{\text{molecules}}{\text{unit cell}}\right]$	$\left[\frac{m^2}{s}\right]$	z	a	b	$a_{i,1}$	$a_{i,2}$	$a_{i,3}$	$a_{i,4}$
C_2H_4	22	9.95e−12	2.5	0.7687	0.3651	0.1088	1.4554	0.3063	0.90
C_6H_6	4	2.0e−13	–	–	–	3	0	0	0
C_8H_{10}	4	1.6e−13	–	–	–	3	0	0	0

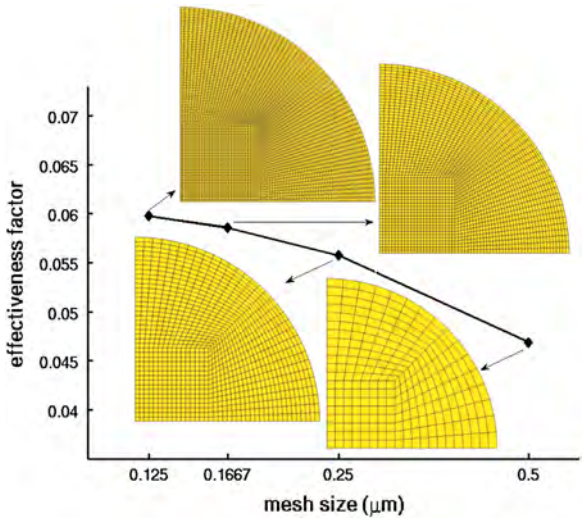

Fig. 3. Effectiveness factor of a catalyst pellet of 10 μm radius composed exclusively by H-ZSM-5 crystal particles as function of mesh size.

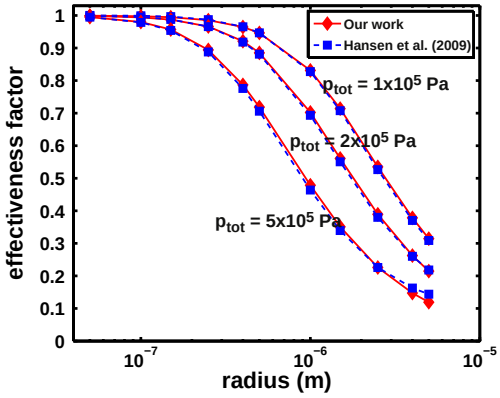

Fig. 4. Effectiveness factor as function of the particle radius for three total gas phase pressures at 653 K and a benzene to ethene ratio of 5. Our 3D model results are shown as diamonds, and the data from Hansen et al. (2009) are shown as squares.

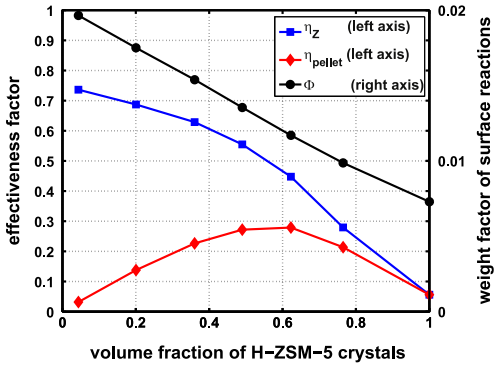

Fig. 5. The effectiveness factors η_{pellet} and $\eta_{\mathcal{Z}}$ versus volume fraction of H-ZSM-5 crystal particles (left axis). Weight factor of surface reactions versus volume fraction of H-ZSM-5 crystal particles (right axis).

0.25 μm is 180224, which is only one eighth of that for mesh size of 0.125 μm, the computational efficiency significantly increases. Thus in the following subsections we chose 0.25 μm as the radial mesh size for the simulations to study effects of volume fraction, size and spatial distribution of H-ZSM-5 crystal particles.

Before investigation on the influence of volume fraction, size and spatial distribution of H-ZSM-5 crystal particles, we first carried out simulations for a single spherical H-ZSM-5 crystal particle for validation. In total 33 simulations have been carried out for this comparison, which include simulations for different crystal size and gas phase pressure. The particle radii of these validation simulations range from 0.05 to 5.0 μm, and their mesh sizes are chosen less than 0.25 μm. It is seen that the effectiveness factor decreases as the crystal radius increases due to the diffusion limitation (Hansen et al., 2009). The results of the effectiveness factor predicted by our 3D model agree well with the results reported by Hansen et al. (2009), as shown in Fig. 4. Note that the surface reactions at the boundaries included in Eq. (26) were neglected for the comparison since they were not considered by Hansen et al. (2009). From Fig. 4, it can be found that the volume average reaction rate of spherical crystal decreases significantly with the increased crystal size, because the reaction kinetics is faster compared to the diffusion mass transfer for crystal particle with larger crystal size. The value of $\eta_{\mathcal{Z}}$calculated from above mesh convergence simulations, as shown in Fig. 3, is below 0.1 when the H-ZSM-5 crystal radius increases up to 10 μm.

4.2. *Effect of volume fraction of crystal particles*

As stated above, the effectiveness factor of a pellet of 10 μm radius, which is composed exclusively by H-ZSM-5 crystals, is low (below 0.1). In order to enhance catalytic performance of the pellet of 10 μm radius, it is natural to increase the volume fraction of meso-pores or macro-pores in the pellet. It is obvious that $\eta_{\mathcal{Z}}$ should increase as the volume of subregion $\mathcal{A}$ increases in a pellet with a given radius. However, the curve of η_{pellet} versus the volume fraction of subregion $\mathcal{A}$ could possess a maximum, where the position is dependent on specific properties of catalyst pellet and reactants. The maximum indicates the optimized catalytic performance of a pellet with a given size.

We then investigated the effect of volume fraction of H-ZSM-5 crystal particles on η_{pellet}. In this simulation, each H-ZSM-5 crystal particle occupies 8 neighboring mesh units. Fig. 5 shows the simulation results of η_{pellet} and $\eta_{\mathcal{Z}}$ versus volume fraction of H-ZSM-5 crystals at temperature of 653 K. It is evident that the curve of η_{pellet} has a maximum when the volume fraction of H-ZSM-5 crystals is 0.623, while $\eta_{\mathcal{Z}}$ decreases monotonically within creasing volume fraction of H-ZSM-5 crystal particles. This implies that the catalyst pellet shows best catalytic performance at volume fraction of H-ZSM-5 crystal particles of 0.623.

The diffusion resistance in subregion $\mathcal{A}$ increases as the volume fraction of the region $\mathcal{Z}$ increases. Fig. 6 represents the distributions of species partial pressures and reaction rate at different volume fractions of H-ZSM-5 crystals. It is seen that pressure variations of species within subregion $\mathcal{A}$ increases as the volume fraction of region $\mathcal{Z}$ increases, describing the relation between the diffusion resistance in subregion $\mathcal{A}$ and the volume fraction of region $\mathcal{Z}$. The phenomenon could be understood due to the fact that the increasing volume fraction of the region $\mathcal{Z}$ enhances both the steric diffusion-hindrance and the component absorbability. It is noted that higher absorbability of species could increase the diffusion resistance of species in a multi-porous pellet. With the increase in the diffusion resistance in the subregion $\mathcal{A}$, reaction rate in region $\mathcal{Z}$ decreases monotonically, which is consistent with the change of $\eta_{\mathcal{Z}}$. However, the curve of η_{pellet} does not change monotonically, because it is determined not only by the reaction rate, but also by the total volume of region $\mathcal{Z}$.

Since the diffusion resistance in subregion $\mathcal{A}$ is considerably smaller than that in region $\mathcal{Z}$, surface reaction of the pellet is worthy of attention. In order to describe conveniently the effect of the surface reaction compared with volume reaction, we defined a

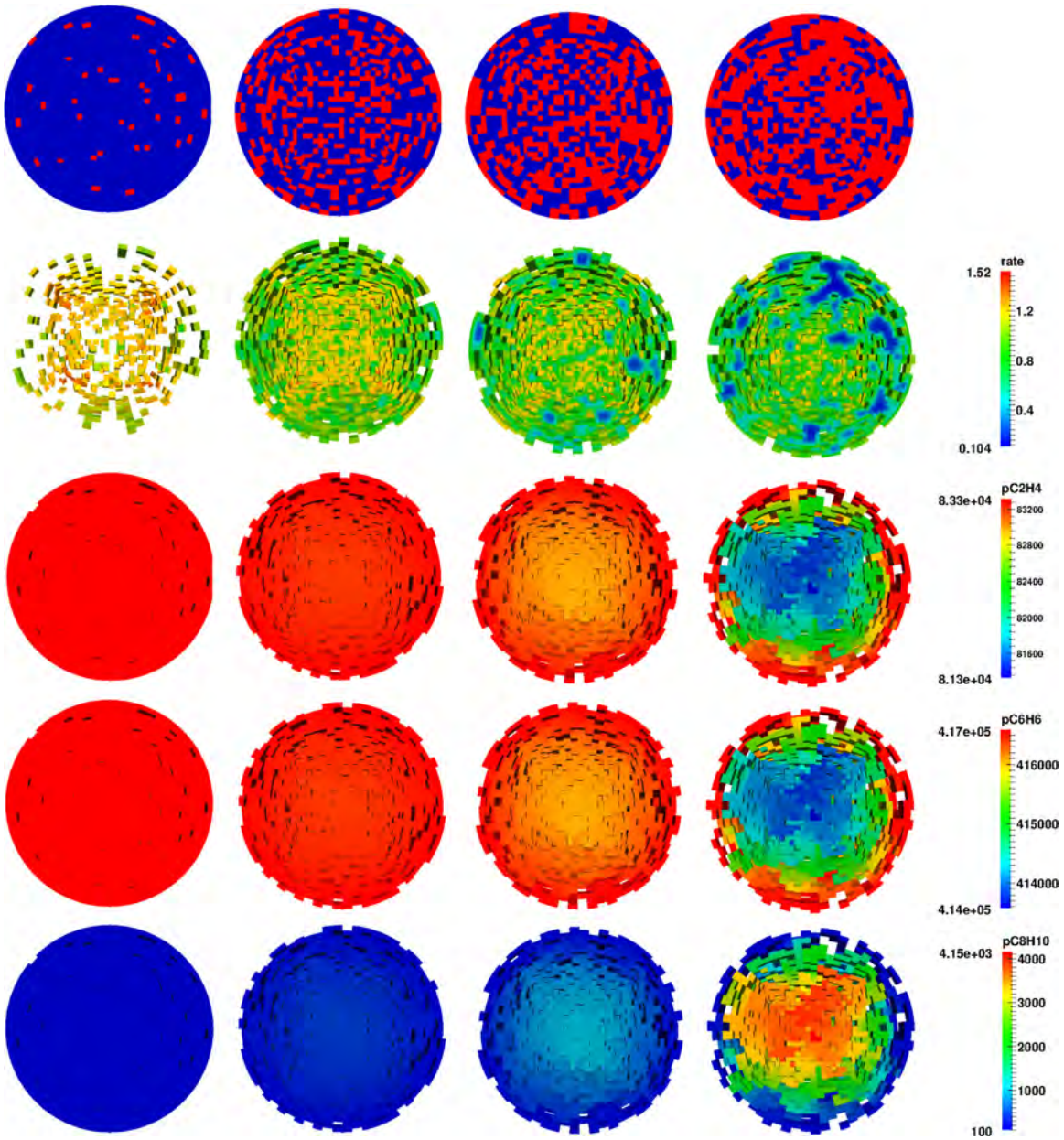

Fig. 6. Distributions of crystal particles over cross sections of catalyst pellets (in first row), distributions of reaction rate of C_8H_{10} in H-ZSM-5 crystal region (in second row), and distributions of pressures of C_2H_4, C_6H_6 and C_8H_{10} in support region (in third, fourth, and fifth row, respectively).In first row, the crystal particles are plotted in red color, while the support region is plotted in blue color. The plots shown in the same column correspond to the same volume factor of H-ZSM-5 crystals. The values of volume fraction of first, second, third and fourth column are 0.043, 0.360, 0.490 and 0.623, respectively. (For interpretation of the references to color in this figure legend, the reader is referred to the web version of this article.)

weight factor (in dimensionless)

$$\phi \equiv \frac{c_u^s \int_{S_\mathcal{Z}} r_{C8H10}\, dS}{c_u^v \int_{V_\mathcal{Z}} r_{C8H10}\, dV} \tag{28}$$

ϕis dependent on the problem itself, i.e. the capacity of diffusion mass transfer in subregion $\mathcal{A}$ and reaction kinetics of H-ZSM-5 crystal. Fig. 5 shows the curve of ϕ versus volume fraction of H-ZSM-5 crystals obtained from simulations. Φ decreases monotonically with increasing volume fraction of H-ZSM-5 crystals, which represents that higher diffusion resistance in the support region decreases the importance of surface reaction. The low values of ϕ calculated from simulations, below 0.02, indicate that the volume reaction is more important than surface reaction for the alkylation of benzene in our constructed H-ZSM-5 pellet.

4.3. Effect of crystal particle size

In the simulations above, we explored the effect of the volume fraction of the crystal particles within a catalyst pellet on the catalytic performance. The size of the crystal particles in these simulations was set as 0.5 μm. For convenience, we call these crystal particles *normal crystal particles*. From Fig. 4 it could be found that the catalytic performance of catalyst pellet composed of normal crystal particles is influenced to a certain degree by the internal diffusions within the single crystal particle. So it may be expected that the effectiveness factor increases with the reduced crystal particle size. To study the effect of the crystal particle size, we then introduce fine crystal particles which have a size of 0.25 μm, i.e. half of that of the normal crystal particles. Fig. 7 demonstrates the crystal particle distributions and reaction rate

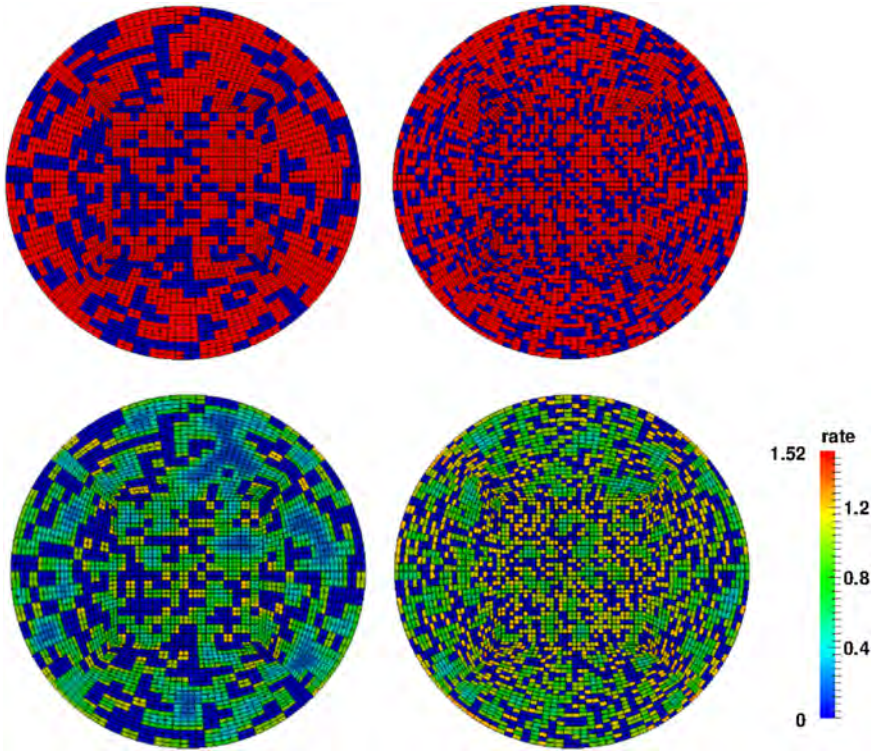

Fig. 7. The crystal particle distributions and reaction rate distributions over cross sections of catalyst pellets with volume fraction of H-ZSM-5 crystal particles of 0.62. The distributions of the pellet composed by normal crystal particles (first column) and by fine crystal particles (second column). The first row shows the distributions of crystal particles (the crystal particles are plotted in red, while the support region is plotted in blue), and the second row shows the reaction rate distributions. (For interpretation of the references to color in this figure legend, the reader is referred to the web version of this article.)

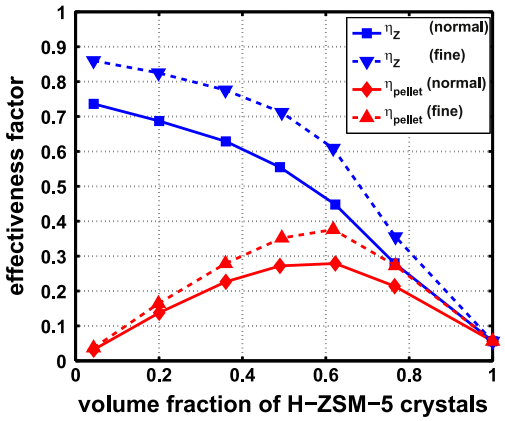

Fig. 8. Effectiveness factor as a function of volume fraction of H-ZSM-5 crystal particles for both normal and fine crystal particles.

distributions over cross sections of the catalyst pellet, which has a volume fraction of H-ZSM-5 crystal particles of 0.62. Our simulations verified that the catalyst pellet composed by fine crystal particles has higher effectiveness factor than that composed by normal crystal particles, as shown in Figs. 7 and 8. Since it is easy to obtain relatively large inter-connected subregions in crystal regions inside a catalyst pellet with larger crystal particles, the diffusion resistance in the crystal region inside pellet composed by normal crystal particle is usually larger than that composed by fine crystal particle. And catalyst pellet composed by fine crystal particles, mean while, could create more complex support region which leads to higher diffusion resistance in the support region. Our simulations suggest that the internal diffusion resistance within the crystal region is decisive for the effectiveness factor of the catalyst pellet, as shown in Fig. 8. This is not surprised since the diffusion coefficient of crystal regions is much lower than that of support regions, and thus the diffusion resistance in the crystal region is highly sensitive to the size of crystal particles.

4.4. *Effect of spatial distribution of crystal particles*

In designing catalyst pellet, the spatial distribution of crystal particles is of great importance. An optimal distribution of crystal particles inside catalyst pellet will improve the catalytic performance, because it can reduce the connection complexity of the support region, and enhance the diffusion to the connected crystal regions. In this section, we studied the effect of the spatial distribution of crystal particles. As presented in Fig. 9, three different distributions of normal crystal particles were considered: *outer distribution, random distribution* and *alternate distribution*. The outer distribution means all normal crystal particles are randomly located in the outer surface of the catalyst pellet. The random distribution means all normal crystal particles are randomly located inside the catalyst pellet. For the alternate distribution normal crystal particles are alternately located in the layers of catalyst pellet. Here, the pellet is decomposed into 20 layers, and the crystal particles are randomly located in the odd layers. In all three distributions, the support regions are assumed to be inter-connected. Our simulations indicate that, as shown in Figs. 9 and 10, the effectiveness factor of outer distribution deviates significantly from that of the other two distributions when the volume fraction of H-ZSM-5 crystal particles is increased. This could be ascribed to two reasons: (1) when the volume fraction of crystal particles increases, the crystal particles form a larger inter-connected crystal region at the outer layer of the pellet, which leads to a high internal diffusion resistance in the crystal region, as can be seen from the rate distribution depicted in Fig. 9; (2) In the outer layer of the pellet, the support region is scattered, which leads to the loss of connections to the out surface of the catalyst pellet, which in turn means a higher diffusion

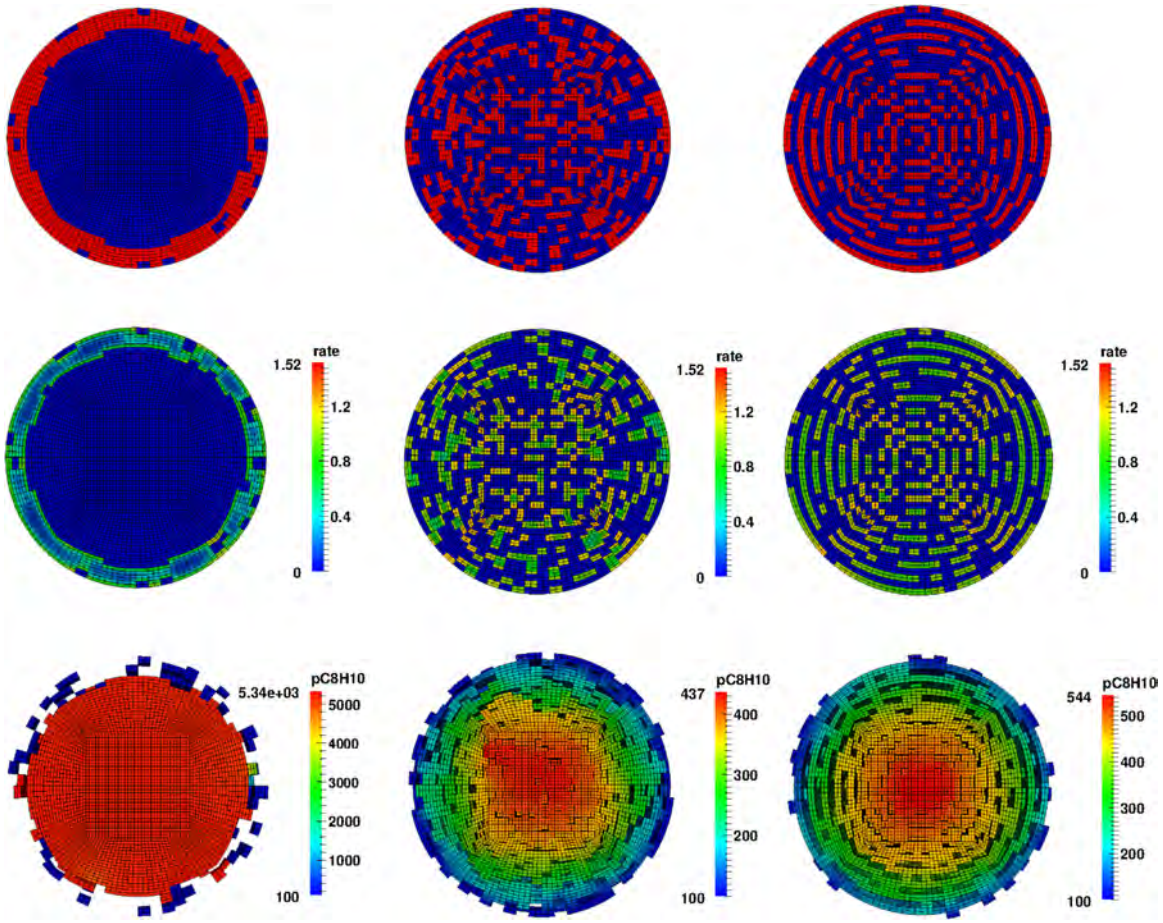

Fig. 9. The spatial distributions of crystal particles (in first row) and reaction rate distributions (in second row) over cross sections of catalyst pellets, and pressure distribution of C_8H_{10} in support region (in third row). All catalyst pellets have volume fraction of H-ZSM-5 crystal particles of 0.36. The crystal particles demonstrate the outer distribution (the first column), random distribution (the second column), and alternate distribution (the third column) in the catalyst pellets. In the first row, the crystal particles are plotted in red, while the support region is plotted in blue. (For interpretation of the references to color in this figure legend, the reader is referred to the web version of this article.)

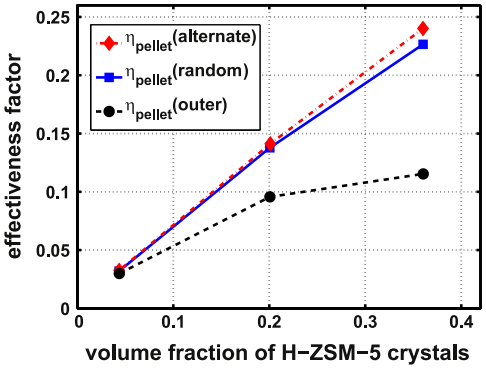

Fig. 10. Effectiveness factor for catalyst pellets with different spatial distribution of crystal particles.

resistance in the support region. This can be evidenced by the high pressure of C_8H_{10} in Fig. 9. Catalyst pellet shows a quite different performance when the crystal particles show the alternate distribution. All crystal particles, in the case of alternate distribution, have at least two faces connected with support region. Our simulations indicate that the alternate distribution has the best catalytic performance when the volume fraction of crystal particles is lower than 0.36 (see Fig. 10). We argued that, however, this distribution is quite artificial and the production of this type of distribution might be difficult in reality. But our purpose here is just to illustrate the applicability of the multi-region model approach. The random distribution is also a better choice in terms of the effectiveness factor of catalyst pellet. On one hand it has very close catalytic performance like alternate distribution (see Fig. 10), and on the other hand it could easily produce high volume fraction of crystal particles (see Figs. 5, 6 and 8). Furthermore, catalyst pellet in reality mostly has random distribution of the crystal particles. Anyway, from our simulations, it can be participated that to optimize the spatial distribution of the crystal particles, one has to consider the compromise of the diffusion resistances in both crystal and support regions to achieve maximum catalytic performance.

4.5. The solver efficiency

The different resistances in subregion $\mathcal{A}$ and region $\mathcal{Z}$ affect the sizes of time steps of their ODE systems. In our simulations, both relative and absolute tolerances of ODE systems were set to the same value $1.0e-14$. The corresponding time steps $dt_{\mathcal{Z}}$ and $dt_{\mathcal{A}}$ were automatically controlled by the program based on the given tolerances. For the simulations with radial mesh size of 0.25 μm, the difference between $dt_{\mathcal{Z}}$ (about $9.e-9s$) and $dt_{\mathcal{A}}$ (about $2.e-5s$) is about 3–4 orders of magnitude. So using the approach based on quasi-stationary state assumption could significantly improve the solving efficiency. In order to show the details of evolution of ODE systems, the results of a multi-porous pellet with 0.043 volume fraction of H-ZSM-5 crystals are shown in Figs. 11 and 12. In this simulation,$dt_{coupling}$ was set to 0.001 s, and the integration time of

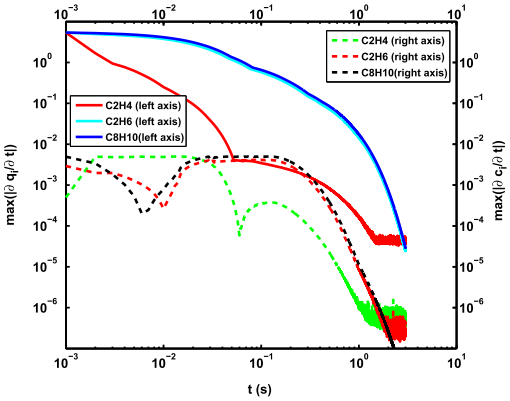

Fig. 11. Simulated $\mathbf{max}\left(\left|\frac{\partial q_i}{\partial t}\right|\right)$ as a function of time (left axis).Simulated $\mathbf{max}\left(\left|\frac{\partial c_i}{\partial t}\right|\right)$ as a function of time (right axis).

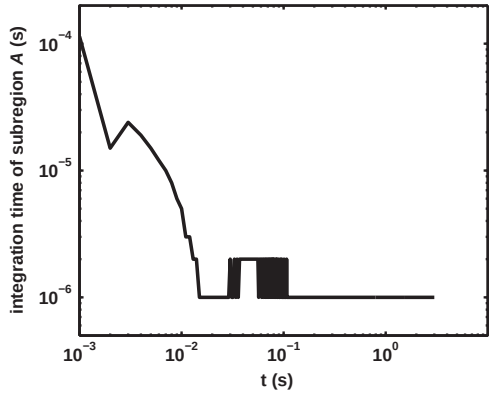

Fig. 12. Integration time of subregion $\mathcal{A}$ at each coupling interval as a function of time.

ODE systems of subregion $\mathcal{A}$was required not less than 1.0e−6 s. That is to say, the integration time of subregion $\mathcal{A}$ is controlled with the range from 1.0e−6 s to 0.001 s at every coupling interval. Based on the quasi-stationary state assumption, the integration time of $\mathcal{A}$ will be actually far smaller than 0.001 s in most steps. This is achieved by setting a criterion of $\left|\frac{\partial c_i}{\partial t}\right|$ (denoted by σ here). If all values of $\left|\frac{\partial c_i}{\partial t}\right|$ in subregion $\mathcal{A}$ are smaller than σ, the integration of ODE systems of subregion $\mathcal{A}$ should be normally terminated at current coupling interval.The value of σshould be set according to the problem itself, and in this simulation σ is set to 0.005. Fig. 11 shows that the curves of $\max\left(\left|\frac{\partial q_i}{\partial t}\right|\right)$ decrease monotonically within the first one second. The integration time of region $\mathcal{Z}$ is equal to $dt_{coupling}$ at every coupling interval. However, the integration times of subregion $\mathcal{A}$ are smaller than $dt_{coupling}$ since $\max\left(\left|\frac{\partial c_i}{\partial t}\right|\right) < \sigma$ is satisfied under the quasi-stationary state assumption (see Figs. 11 and 12). As shown in Fig. 12, the integration time of subregion $\mathcal{A}$ decreases from 1.14e−4 s, and reaches the minimum setting time (1.0e−6 s) when the whole system evolves about 0.1 s. In this simulation, the whole system takes about 3 s to reach stationary state, and more than 90% of the integrations of the subregion $\mathcal{A}$requires far fewer time than region $\mathcal{Z}$. Considering small value of $dt_{\mathcal{Z}}$ (about 9.e−9 s), the reduced integration time of subregion $\mathcal{A}$ significantly improves the solving efficiency.

5. Conclusions

A multi-region model based on the unified Maxwell–Stefan diffusion theory is developed to study the catalytic performance of a porous catalyst pellet formed with micro-porous crystal particles and meso/macro-porous support. This model can be considered as a derivative from the multi-scale approach which could effectively reveal the essence of diffusion–reaction processes that are directly related to the molecule-molecule and molecule-pore wall interactions within the catalyst pellet. Based on the multi-region model, the effects of the volume fraction, size, and spatial distribution of micro-porous crystal particles on the effectiveness factor of the catalyst pellet could be investigated via computational simulations.

The complicated processes in a catalyst pellet including (surface) chemical reactions, bulk diffusion, Knudsen diffusion, surface diffusion and Darcy flow exhibit a multi-scale nature in time. The corresponding multi-scale PDE systems are converted to ODE systems via discretization by use of finite volume method (FVM). The resulting ODE systems are solved by reduced storage matrix method. The value of the time interval for updating the coupling mass fluxes between catalyst support region and micro-porous crystal region determines the efficiency and accuracy of the solution. A loose criterion for the ODE system of the support region that connected to pellet's boundary is used to improve the solution efficiency.

As an example of applications, the model was first validated against the data of the alkylation of benzene over a single porous catalyst pellet formed with H-ZSM-5 crystal particles by Hansen et al. (2009), which suggests a good agreement between our results with their data. Then the efficiency of this model is further demonstrated by studying the effects of the volume fraction, size, and spatial distribution of the H-ZSM-5 crystal particles on the effectiveness factor of a catalyst pellet with radius of 10 μm. The results show that the largest effectiveness factor, which indicates the best catalyst performance, is found at volume fraction of 0.623 for a catalyst pellet with a random spatial crystal distribution. It also shows that the crystal particle size and spatial distribution of crystal particles play important roles in controlling the internal diffusion resistance within crystal region and thus determines the catalytic performance of catalyst pellet. Since the difference of time step between H-ZSM-5 crystal region and catalyst support region is in 3–4 orders of magnitude, the multi-region model developed in this work is therefore a potential bottom to up tool for reaction-diffusion processes inside a catalyst pellet exhibiting multi-scale time characteristic. The possible applications include rational catalyst design for zeolite based catalyst encountered in many industrial applications.

Acknowledgment

This work is funded by Projects 21406217 and 91334205 supported by the National Natural Science Foundation of China. We thank Niels Hansen for the help in calculations of H-ZSM-5 crystal. We thank two anonymous reviewers for their helpful comments on earlier drafts of this paper.

References

Brown, P.N., Hindmarsh, A.C., 1989. Reduced storage matrix methods in stiff ODE systems. J. Appl. Math. Comp 31, 40–91.
Chen, N.Y., Degnan Jr., T.F., Smith, C.M., 1994. Molecular Transport and Reaction in Zeolites: Design and Application of Shape Selective Catalysis. VCH, New York.
Gear, C.W., 1971. Numerical Initial Value Problems in Ordinary Differential Equations. Prentice-Hall, Englewood Cliffs, New Jersey.
Hansen, N., Keil, F.J., 2012. Multiscale modeling of reaction and diffusion in zeolites: from the molecular level to the reactor. Soft Mater. 10 (1-3), 179–201.
Hansen, N., Keil, F.J., 2013. Multiscale approaches for modeling hydrocarbon conversion reactions in zeolites. Chem. Ing. Tech. 85, 413–419.
Hansen, N., Krishna, R., van Baten, J.M., Bell, A.T., Keil, F.J., 2009. Analysis of diffusion limitation in the alkylation of benzene over H-ZSM-5 by combining quantum chemical calculations, molecular simulations, and a continuum approach. J. Phys. Chem. C 113, 235–246.
Hegedus, L.L., Pereira, C.J., 1990. Reaction engineering for catalyst design. Chem. Eng. Sci. 45, 2027–2044.

Hinderer, J., Keil, F.J., 1995. Diffusion and reaction in composite catalysts. Hung. J. Ind. Chem. 23, 207–213.
Kärger, J., Ruthven, D.M., 1992. Diffusion in Zeolites and Other Microporous Solids. John Wiley & Sons INC, New York.
Keil, F.J., Hinderer, A.R., Garayhi, A.R., 1999. Diffusion and reaction in ZSM-5 and composite catalysts –a Monte-Carlo approach applied to the methanol-to-olefin synthesis. Catal. Today 50, 637–650.
Keil, F.J., 2012. Multiscale modelling in computational heterogeneous catalysis. Top. Current Chem. 307, 69–108.
Keil, F.J., 2013. Complexities in modeling of heterogeneous catalytic reactions. Comput. Math. Appl. 65, 1674–1697.
Kerkhof, P.J.A.M., 1996. A modified Maxwell–Stefan model for transport through inert membranes: the binary friction model. Chem. Eng. J. 64, 319–343.
Kortunov, P., Vasenkov, S., Karger, J., Fe Elia, M., Perez, M., Stocker, M., Papadopoulos, G.K., Theodorou, D., Drescher, B., Mcelhiney, G., Bernauer, B., Krystl, V., Kocirik, M., Zikanova, A., Jirglova, H., Berger, C., Glaser, R., Weitkamp, J., Hansen, E.W., 2005. Investigations of molecular diffusion in FCC catalysts. Diffus. Fundam. 2, 97.1–97.2.
Krishna, R., 1993. Problems and pitfalls in the use of the fick formulation for intraparticlediffusion. Chem. Eng. Sci. 48, 845–861.
Krishna, R., Wesselingh, J.A., 1997. The Maxwell–Stefan approach to mass transfer. Chem. Eng. Sci. 52, 861–911.
Krishna, R., van Baten, J.M., 2009a. An investigation of the characteristics of Maxwell–Stefan diffusivities of binary mixtures in silica nanopores. Chem. Eng. Sci. 64, 870–882.
Krishna, R., van Baten, J.M., 2009b. Unified Maxwell–Stefan description of binary mixture diffusion in micro- and meso-porous materials. Chem. Eng. Sci. 64, 3159–3178.
Lim, J.Y., Dennis, J.S., 2012. Modeling reaction and diffusion in a spherical catalyst pellet using multicomponent flux models. Ind. Eng. Chem. Res. 51, 15901–15911.
Myers, A.L., Prausnitz, J.M., 1965. Thermodynamics of mixed-gas adsorption. AIChE J. 11, 121–127.
Radhakrishnan, K., Hindmarsh, A.C., 1993. Description and use of LSODE, the Livermore Solver for Ordinary Differential Equations. NASA Reference Publication 1327, LLNL Report UCRL-ID-113855.
Reid, R.C., Prausnitz, J.M., Poling, B.E., 1987. The Properties of Gases and Liquids. MacGraw-Hill, New York.
Sahimi, M., 1990. Diffusion, adsorption, and reaction in pillared clays. 1. Rod-like molecules in a regular pore-space. J. Chem. Phys. 92, 5107–5118.
Smit, B., Maesen, T.L.M., 2008. Molecular simulations of zeolites: adsorption, diffusion, and shape selectivity. Chem. Rev. 108, 4125–4184.
Solsvik, J., Jakobsen, H.A., 2011. Modeling of multicomponent mass diffusion in porous spherical pellets: application to steam methane reforming and methanol synthesis. Chem. Eng. Sci. 66, 1986–2000.
Solsvik, J., Jakobsen, H.A., 2012. A survey of multicomponent mass diffusion flux closures for porous pellets: mass and molar forms. Transport Porous Media 93, 99–126.